







# In situ preparation of graphene/polypyrrole nanocomposite via electrochemical co-deposition methodology for anti-corrosion application

Meixiu Li<sup>1</sup> , Xuqiang Ji<sup>1</sup> , Liang Cui<sup>1</sup> , and Jingquan Liu<sup>1,\*</sup> 

<sup>1</sup> College of Materials Science and Engineering, Institute for Graphene Applied Technology Innovation, Qingdao University, Qingdao 266071, China

Received: 16 May 2017

Accepted: 5 July 2017

Published online:

11 July 2017

© Springer Science+Business Media, LLC 2017

## ABSTRACT

Graphene has attracted much attention and triggered extensive anti-corrosion applications due to its excellent electrochemical stability and robust barrier for molecules and ions. In this paper, a novel polypyrrole/reduced graphene oxide (PPy/rGO) nanocomposite was successfully prepared on carbon steel as an efficient protective coating for improving the anti-corrosion property. Graphene oxide (GO) was deposited onto carbon steel via potentiostatic technique, and PPy was obtained simultaneously by oxidation polymerization. Scanning cyclic voltammetry method was adopted to reduce GO into rGO to form PPy/rGO nanocomposite coating. Due to the synergistic effect of PPy and rGO, excellent anti-corrosion performance for carbon steel in simulated seawater was obtained. Impressively, the PPy/rGO-coated carbon steel showed 7.05 times higher corrosion resistance than that of bare carbon steel and revealed the excellent protection efficiency above 95.9%. The anti-corrosion mechanism of the PPy/rGO coating was also proposed. Our results suggested that the PPy/rGO composite coatings could serve as effectively protectors for anti-corrosion of seawater, therefore, they could envision potential applications in naval architecture and ocean engineering.

## Introduction

The protection of metals from corrosion plays an important role in industrial and academic topic. Conducting polymers have been proved to be the environmental friendly materials with excellent anti-corrosion capability [1]. Many conducting polymers, such as polyaniline and polypyrrole (PPy), have been

widely used as either protective coating or anti-corrosion film inhibitors because of its easy processability, excellent environment stability and interesting redox properties associated with the chain of nitrogen [2, 3]. Among the conducting polymers, PPy has attracted increasing attention due to its excellent electrical properties, good environmental stability and ease of preparation, which enable its

Address correspondence to E-mail: jliu@qdu.edu.cn

wide applications in electronic devices, rechargeable batteries and supercapacitors, solid electrolytes for capacitors, sensors and corrosion protection materials [4–9]. In recent years, a lot of studies have revealed that PPy coating has well protective behavior on active metals [10–12]. Lei et al. [13] synthesized PPy films electrochemically on copper, which exhibited good adhesivity and corrosion-resistant behavior in 3.5% NaCl solution. PPy/carbon nanotubes composites have been successfully prepared as anti-corrosion material for carbon steel in 3.5% NaCl solution and exhibited good anti-corrosion protecting ability [12]. In spite of the fact that many studies about the anti-corrosion ability of PPy have been performed, development of facile and efficient anti-corrosion coatings is still in great demand. In addition, the dopant for PPy to obtain new composites is usually required in order to obtain enhanced conductivity and permeability. The increasing demand for corrosion-inhibiting coating motivates the researchers to develop new materials with high corrosion-resistant properties for applications in naval architecture and ocean engineering [14].

In the past few years, extensive researches on graphene have been performed in the fields of applied physics, chemistry, materials science and engineering because of its outstanding mechanical and hydrophobic characteristics, good thermal and electrical conductivity and highly accessible surface areas, etc. [15–18]. It has been reported that graphene can be exploited to be a robust barrier for molecules [19]. The other unique characteristics, such as chemical inertness, excellent thermal and electrical conductivity, remarkable flexibility and impermeability to molecules make graphene a potential anti-corrosion material [20–23]. Bunch et al. [19] demonstrated that a monolayer graphene membrane was impermeable to standard gases including helium. Graphene coating on copper also showed enhanced resistance to electrochemical degradation [24]. It has been proved that graphene coatings on Ni and Cu could serve as barriers to electrochemical corrosion in aqueous media [25].

In this paper, we chose PPy as one dopant for reduced graphene oxide (rGO) to afford a novel polypyrrole/graphene oxide (PPy/GO) nanocomposite on carbon steel surface using a facile one-step potentiostatic technique for anti-corrosion application. PPy/GO was fabricated onto carbon steel surface by the in situ reduction of GO and pyrrole (Py)

monomer via scanning cyclic voltammetry (CV) method. The anti-corrosion performance of the composite coatings with varying PPy content was investigated. The composition and morphology as well as the structure of the coatings were studied using Fourier transform infrared spectroscopy (FTIR), X-ray photoelectron spectroscopy (XPS) and scanning electron microscope (SEM). The anti-corrosion behaviors of the composite coatings were investigated using potentiodynamic polarization measurements, electrochemical impedance spectroscopy (EIS), open-circuit potential ( $E_{ocp}$ ) and Bode plot.

## Experimental section

### Materials

Py (99%, Aladdin) was purified through distillation under vacuum and stored at a temperature less than 5 °C. Sulfuric acid (98%), hydrogen peroxide (30%), potassium persulfate (99.5%), sodium sulfate (99.5%), potassium permanganate (99.5%), phosphorus (V) oxide (98%) and hydrochloric acid (37%) were purchased from Shandong Laiyang Economic and Technological Development Zone Chemical Plant.  $\text{KH}_2\text{PO}_4$  (AR),  $\text{K}_2\text{HPO}_4$  (AR) and high-precision regenerated cellulose dialysis membrane (3500 cutoff) were purchased from Ebioeasy, Shanghai. Graphite micro-powder was donated by Xiamen Knano Graphite Technology Corporation Limited. Sheet-shaped carbon steel was purchased from Jiangsu Miaomiao Water Technology. All the other chemicals were purchased from Heowns and were used without further purification.

### Preparation of PPy/GO nanocomposite coating

The GO was synthesized according to a modified Hummers' method as described in previous report [26]. The as-prepared GO was purified by dialysis in double-distilled water for three days using a 3500-Da cutoff dialysis membrane tube. The GO suspension was dried by vacuum freezing drying to obtain the GO powder. The stable GO suspension (1 mg/mL) was obtained by sonication under ambient conditions for 1 h and then bubbled by  $\text{N}_2$  for 30 min to remove  $\text{O}_2$  in case of Py oxidation.

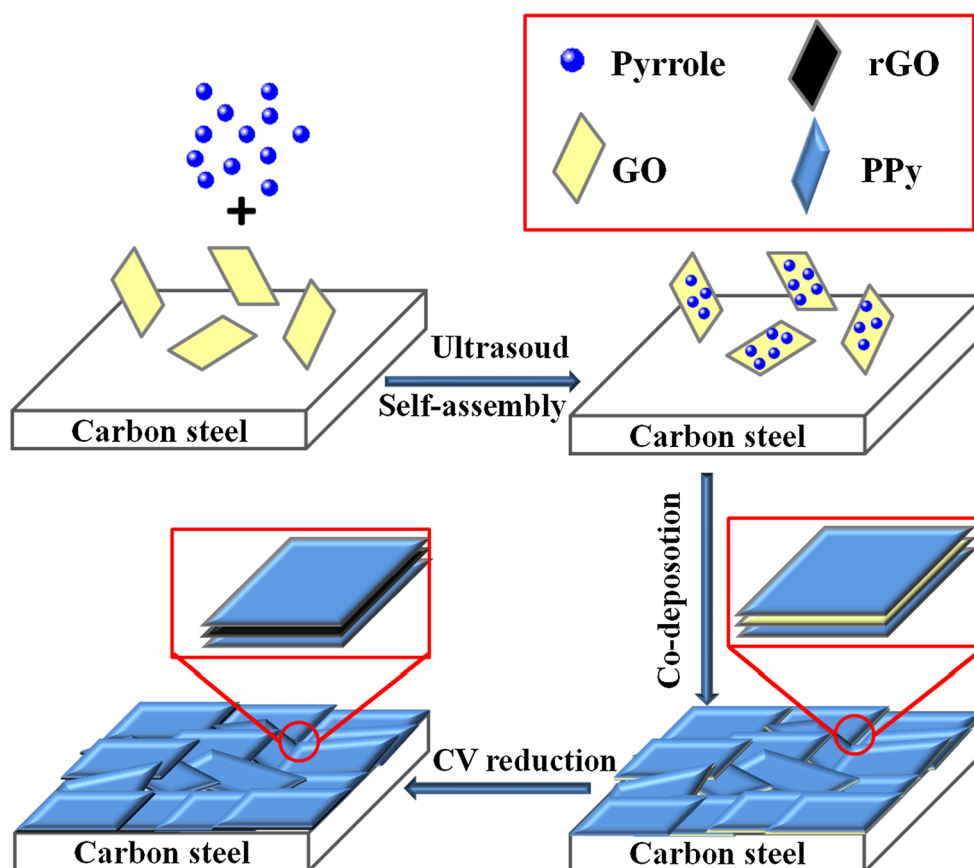
Py (67 mg, 1 mmol) was added into GO suspension (10 mL, 1 mg/mL) and then sonicated under ambient condition for 3 h to obtain the homogeneous GO and Py colloidal suspension. The PPy/GO composite was directly self-assembled on the surface of carbon steel by electrochemical polymerization using the potentiostatic method (Scheme 1). A constant potential of 1.2 V was applied for 20 min to form the PPy/GO composite onto the surface of carbon steel. After self-assembly of PPy/GO nanocomposite coating onto carbon steel surfaces, the carbon steel was carefully rinsed with double-distilled water to remove the adsorbed Py and GO and then was dried under an ultrapure nitrogen stream. The PPy/GO composites coatings with different weight ratios of PPy to rGO (16.7, 33.5 and 83.8, respectively) were prepared from the GO solution (1 mg/mL) containing 0.1, 0.2 and 0.5 M pyrrole, respectively. Accordingly, the PPy/GO composites were simplified as 0.1, 0.2 and 0.5 PPy/GO, respectively. Meanwhile, 0.1, 0.2 and 0.5 PPy/rGO represent the samples prepared by

electroreduction of the corresponding PPy/GO composites, respectively.

### In situ electroreduction of PPy/GO nanocomposite coating

The GO in the PPy/GO composite was reduced by scanning CV method. Nitrogen was bubbled into saturated 0.5 M Na<sub>2</sub>SO<sub>4</sub> solution to remove the O<sub>2</sub>. The reduction reaction was then conducted by CV scanning from -1.5 to 0 V in saturated 0.5 M Na<sub>2</sub>SO<sub>4</sub> for 5 cycles at a scan rate of 10 mV s<sup>-1</sup> until the reduction peak at -1.34 V completely disappeared. The obtained PPy/rGO-coated carbon steel was dried under vacuum at 50 °C for 3 h after rinsing with double-distilled water. For comparison, pure PPy was coated on carbon steel using a solution containing 0.5 M Py monomer and 0.5 M H<sub>2</sub>SO<sub>4</sub> via the same procedure as mentioned above. The pure GO was self-assembled onto the surface of carbon steel from 1 mg/mL GO suspension and reduction using the

**Scheme 1** Schematic for formation of the PPy/rGO nanocomposite coating on carbon steel via electrochemical co-deposition of GO and pyrrole using potentiostatic oxidation technique at 1.2 V and subsequent reduction of GO into rGO by repeating CV scanning from -1.5 to 0 V at 10 mV s<sup>-1</sup>.



same procedure. The mechanism for formation of PPy/GO and PPy/rGO composites is proposed in Scheme 1.

### Characterizations and measurements

The working electrode was prepared by polishing the sheet-shaped carbon steel on emery papers of various grades (1000–5000 grit), followed by rinsing with distilled water and then ethanol under sonication. Both the electrochemical self-assembly and reduction experiments were carried out on a CHI 760D electrochemical workstation (CHI Instruments, Shanghai, China) in a three-electrode cell, with the processed carbon steel as working electrodes, a piece of Pt sheet as auxiliary electrode and an Ag/AgCl (3.0 M NaCl) electrode as reference. The carbon steel was composed of 98.69 Fe, 0.08 C, 0.15 Si, 0.40 Mn, 0.03 P, 0.12 Cr, 0.25 Ni and 0.25 Cu weight percent. The morphology of the coatings was characterized with a SEM (JEOL JSM-7500F). XPS analysis was performed on an Escalab 250 X-ray photoelectron spectroscopy with an Mg K X-Ray source. FTIR analysis was performed on a Tensor 27 from Bruker Corporation. The anti-corrosion performances of different composite coatings on the carbon steel were carried out on a CHI 760D electrochemical workstation (CHI Instruments, Shanghai, China) using the composites coated carbon steel as the working electrode with working area of 1 cm<sup>2</sup>, a Pt sheet as auxiliary electrode and an Ag/AgCl (3.0 M NaCl) electrode as the reference. EIS, potentiodynamic polarization and  $E_{ocp}$  measurement were obtained with the electrochemical workstation at room temperature. EIS measurements were carried out over a frequency range of 10<sup>-2</sup>–10<sup>5</sup> Hz with 5 mV amplitude of sinusoidal potential variation around the open-circuit potential. The potentiodynamic polarization measurements were carried out by scanning from cathodic to the anodic direction ( $E_{ocp} \pm 250$  mV) at a scan rate of 5 mV s<sup>-1</sup>.

### Results and discussion

The procedures for the preparation of PPy/rGO is Scheme 1. The Py monomers are first adsorbed onto the GO surface by electrostatic interaction, followed by the self-assembly and then co-depositing of the Py adsorbed GO onto carbon steel surface via

potentiostatic oxidation technique at a constant potential of 1.2 V. Finally, GO in the nanocomposite is converted into rGO via in situ electroreduction. During the process of electrochemical self-assembly, the anionic GO served as a counterion to be driven onto the carbon steel surface and simultaneously Py monomers were electrochemically polymerized onto the GO nanosheets to form the special ordered PPy/rGO composite coating on the carbon steel.

### Morphology and wettability analysis

The structure and morphology of the PPy, PPy/GO and PPy/rGO nanocomposite were characterized using SEM and the respective images are shown in Fig. 1a–f. The PPy nanostructures showed thin chrysanthemum-like appearance with sub-micrometer dimensions (Fig. 1a, d). Comparatively, the PPy/GO and PPy/rGO composites exhibited typically layered structure and the GO sheets are surrounded by PPy polymer (Fig. 1b, e). For the PPy/GO or PPy/rGO composite, some wrinkles appeared on the surface of the coating, suggesting that GO was successfully modified with PPy nanosheets. After electroreduction, the morphology of the PPy/rGO coating is barely altered as shown in Fig. 1e and f. The SEM images of PPy, PPy/GO and PPy/rGO coatings at high magnifications are shown in Fig. 1d–f. The rGO sheets are covered by PPy polymer, forming an ordered PPy/rGO composite structure. Such structure might provide an appropriate roughness to increase the contact angle to prevent the diffusion of O<sub>2</sub> and H<sub>2</sub>O to the surface of carbon steel, thus, a better anti-corrosion effect should be expected.

The wettability of PPy, PPy/GO and PPy/rGO coatings was also evaluated in terms of water contact angle (CA) measurements, as shown in the inset in Fig. 1. The CA for PPy surface was measured to be 90°, exhibiting a relatively hydrophilic character. The CA of PPy/rGO surface was measured to be 137.5°, which was much higher than that of PPy/GO surface (85.7°) because rGO possesses less hydrophilic groups than GO. It is well known that the CA depends not only on the chemical structures but also on the surface roughness of the coatings [27, 28]. The good hydrophobic property of PPy/rGO should be resulted from the synergistic effect of the special ordered structure and the high CA of the PPy/rGO coating. The coatings with a high CA can be expected



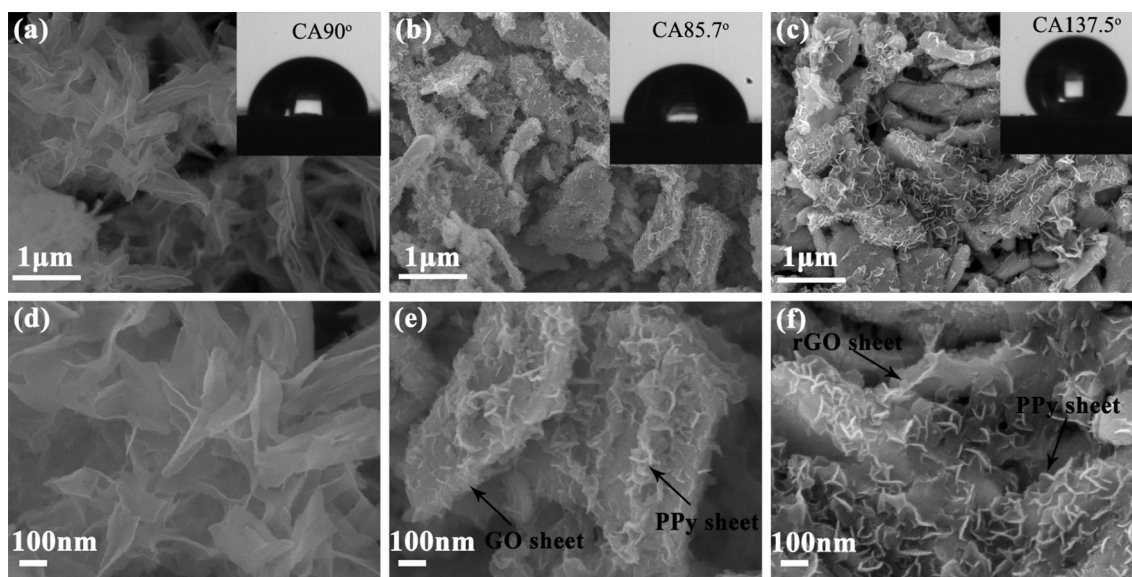


**Figure 1** SEM images of PPy (a, d), PPy/GO nanocomposite coating (b, e) and PPy/rGO nanocomposite coating (c, f) at low and high magnifications, respectively (*inset* corresponding static water contact angles).

to prevent the absorption and diffusion of water and thus provide a better anti-corrosion effect.

### Preparation of rGO/PPy coatings

The PPy/GO composite was self-assembled onto the carbon steel surface by the potentiostatic technique and the current–time curve is shown in Fig. 2a. It can be seen that the plot exhibited three stages: a fast initial decrease to a minimum in the first 5 s, followed by a slower increase till 800 s, and then a gradual plateau level appeared at 1000 s. The initial current decrease was probably due to the insulativity of pyrrole and GO to the electrolyte solution. In the second stage, it could be noted that the oxidation current was gradually increased with time, indicating that the electrochemical polymerization of pyrrole on the carbon steel was successful. When the deposition time reached 800 s, the oxidation current came to a saturated value of approximately 1.68 mA, suggesting that the electrochemical polymerization on the carbon steel surface reached a balance and the PPy/GO coating was formed at constant current and potential conditions. The current–time plot showed the occurrence of pyrrole polymerization process and composites formation in an incubation period of approximately 1200 s at a constant potential of 1.2 V.

To increase the hydrophobicity of the nanocomposite coatings, GO in the PPy/GO was reduced by repeating CV scanning from  $-1.5$  to  $0$  V in  $N_2$

saturated  $0.5$  M  $Na_2SO_4$  solution at a scan rate of  $10$  mV  $s^{-1}$  for 5 cycles. The CV curves for the electroreduction of PPy/GO nanocomposite coatings are shown in Fig. 2b. Interestingly, it could be seen that a notable reduction peak appeared at about  $-1.34$  V in the first scanning cycle and then weakened obviously in the next few cycles and finally disappeared completely after five cycles. It can be concluded that GO in the composite coating was effectively reduced by the electrochemical process. The reduction peak should be resulted from the reduction of the oxygen-containing groups, such as  $-OH$  and  $-COOH$  in the PPy/GO coating [29, 30]. The reduction potential of GO is consistent with those previous reported [31].

### FTIR and XPS analysis

FTIR measurements were carried out to demonstrate the successful preparation of PPy/rGO nanocomposite and the spectra of GO, PPy, PPy/GO and PPy/rGO are shown in Fig. 3a. In the spectrum of GO, the peak at  $1722$   $cm^{-1}$  can be attributed to the  $C=O$  stretching of carbonyl. The peaks observed at  $1402$  and  $1233$   $cm^{-1}$  represent the  $O-H$  deformation and  $C-OH$  stretching vibration, respectively. The peak at  $1062$   $cm^{-1}$  should be attributed to the characteristic  $C-O$  stretching vibration of epoxide group [32]. The peaks at  $1548$ ,  $1461$  and  $911$   $cm^{-1}$  should be assigned to the  $C-C$ ,  $C-N$  and  $C-H$  stretching vibration in the pyrrole ring, respectively. The peaks at  $1165$  and

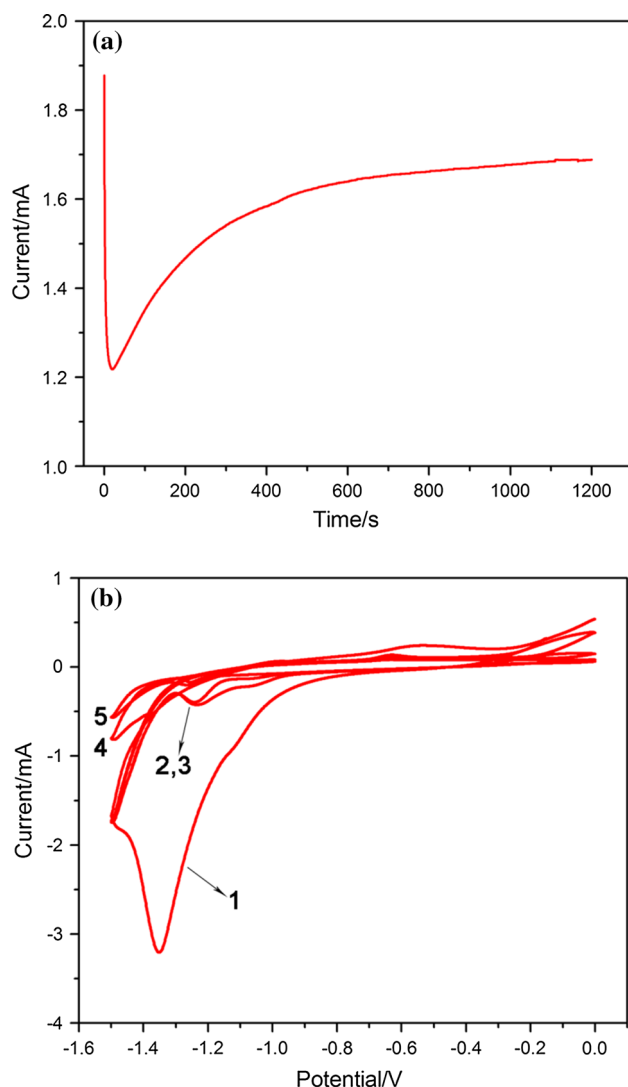


**Figure 2** **a** Current–time plot for PPy/GO coating formation using potentiostatic technique (potential, 1.2 V; pyrrole, 0.2 M; GO, 1 mg/mL). **b** CVs of electrochemical reduction of GO in the PPy/GO composite coating into rGO at  $10 \text{ mV s}^{-1}$  in 0.5 M  $\text{Na}_2\text{SO}_4$  for 5 cycles.

$1072 \text{ cm}^{-1}$  pertain to the C–H in-plane deformation vibration of the PPy ring. The peak at  $1632 \text{ cm}^{-1}$  is due to the C=C backbone stretching. In PPy/GO spectrum, the characteristic peaks of PPy appeared at  $1557$  and  $1465 \text{ cm}^{-1}$ , suggesting the presence of PPy in the PPy/GO. As reported before, the peak assigned to the C=O in the PPy/GO coating down-shifted to  $1709 \text{ cm}^{-1}$ , which should be due to the  $\pi$ – $\pi$  interactions and hydrogen bonding between the GO layers and aromatic PPy rings [33]. In addition, the peak at  $1072 \text{ cm}^{-1}$  due to C–H in-plane vibration of PPy ring shifted to  $1048 \text{ cm}^{-1}$  and the peak at

$911 \text{ cm}^{-1}$  owing to C–H stretching vibration as mentioned earlier shifted to  $923 \text{ cm}^{-1}$  [34]. These peak shifts revealed the chemical environment change as a result of the GO doping into PPy. These peak shifts confirmed that PPy and GO components have been well combined with each other in the coating. As evidenced by the PPy/rGO spectrum shown in Fig. 3a, the peaks resulted from the oxygen functional groups were significantly weakened after the electrochemical reduction, indicating that most GO nanosheets have been reduced into rGO.

XPS analysis was also used to confirm the reduction of GO in the as-prepared PPy/GO coatings. In Fig. 3b, the peak at 400 eV in the survey spectra for PPy/GO and PPy/rGO composite coatings indicated the existence of PPy distributed on the surface of rGO sheets [35]. The presence of the elements C, N and O in the coating was evidenced by the C1s, N1s and O1s peaks at 285, 400 and 531 eV as shown in Fig. 3b. The C/O ratio of PPy/GO was 0.81, and after electrochemical reduction the ratio of PPy/rGO was increased to 1.67, indicating that most GO in PPy/GO was successfully reduced into rGO by CV scanning. As shown in Fig. 3c, the C1s narrow scan spectrum of the PPy/GO composite can be deconvoluted into four Lorentzian peaks with different binding energies at 284.1, 285.2, 286.6 and 288.1 eV, which should be attributed to C–C, C–N, C–O and C=O, respectively [36]. The C1s peaks should be resulted from C–N groups from PPy, suggesting the successful doping of PPy. The C1s peak at 286.9 eV in deconvoluted spectrum for C–O functionality of PPy/rGO (Fig. 3d) decreased significantly, indicating the successful reduction of GO during the electrochemical CV reduction process. It can be concluded that C–O and C=O functionality have been substantially removed after electrochemical reduction [37].

### Potentiodynamic polarization plots analysis

The potentiodynamic polarization measurement was also carried out to investigate the anti-corrosion performance of different composite coatings in 3 wt% NaCl solution, and the results are shown in Fig. 4a. The carbon steel was immersed in the NaCl solution until the potential reached an equilibrium to obtain  $E_{\text{ocp}}$ . The potentiodynamic polarization plots were obtained for a potential range from  $-250$  to  $250 \text{ mV}$  relative to  $E_{\text{ocp}}$ . It can be seen from Fig. 4a that the bare carbon steel displayed an oxidation peak at

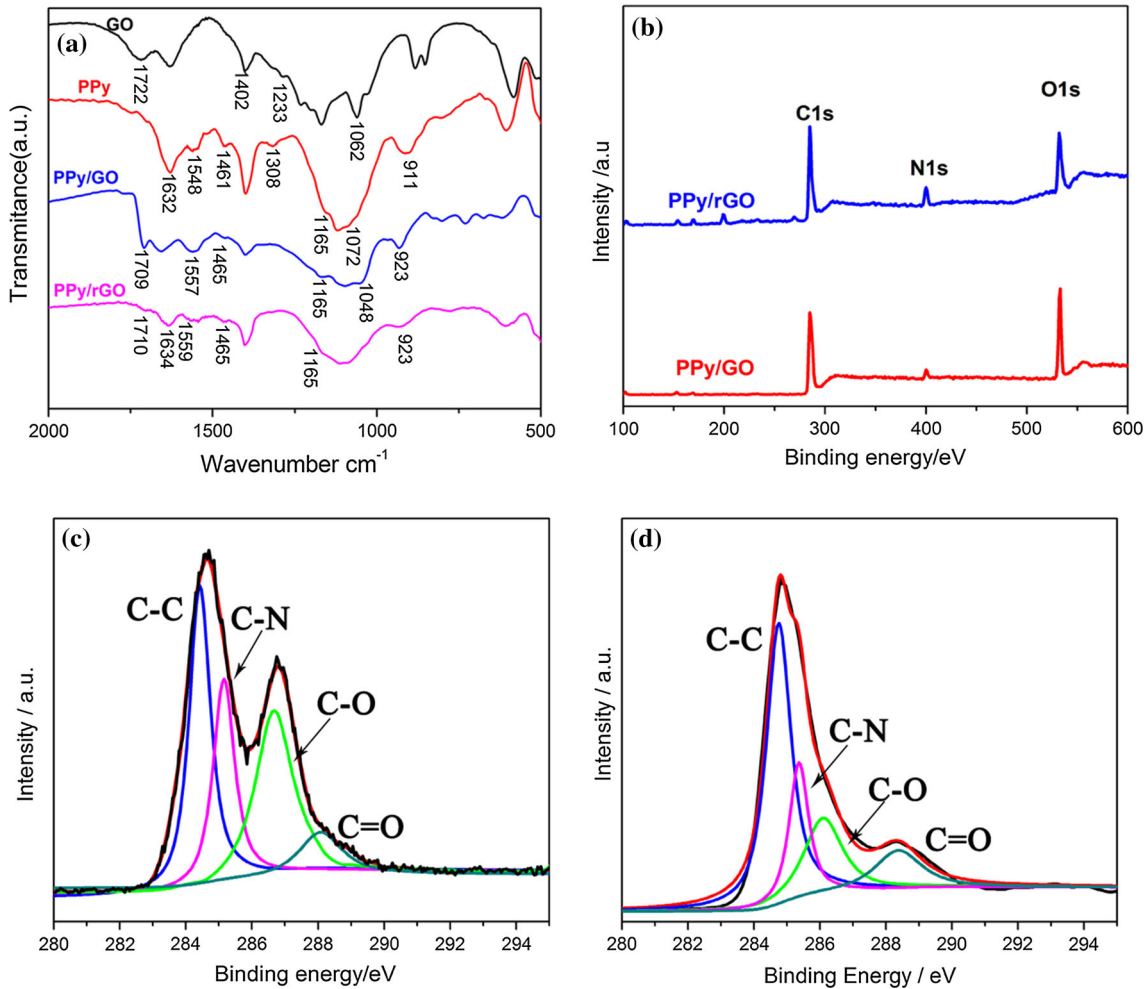


**Figure 3** **a** FTIR spectra of GO, PPy, PPy/rGO and PPyrGO. **b** Survey spectra of PPy/rGO and PPyrGO nanocomposite; **c** deconvoluted C1s XPS spectrum of PPy/rGO; **d** deconvoluted

C1s XPS spectra of PPyrGO (the *black curves* in **c** and **d** are experimental data, and the *red curves* represent the four deconvoluted Lorentzian peaks).

about  $-0.65$  V under anodic polarization due to its dissolution in NaCl solution media. However, no oxidation peaks can be observed from the polarization plot of the carbon steel coated with PPy, rGO and PPy/rGO, indicating their good impermeable performances. In addition, the corrosion currents for the carbon steel coated with rGO, PPy or PPy/rGO were less than that of bare carbon steel (Fig. 4b). The polarization plots of PPy or rGO alone exhibited larger corrosion current and higher corrosion potential than that of PPy/rGO. This is probably due to the porous structure of PPy or rGO, through which  $H_2O$ ,  $O_2$  and  $Cl^-$  can pass through and access the carbon steel surface, subsequently causing the corrosion. For PPy/rGO composite coatings, the impermeability performance was significantly enhanced probably

due to the decreased coating porosity and increased tortuosity of diffusion pathways as a result of the rGO doping [38, 39].

The quantitative analysis of the potentiodynamic polarization was also investigated, and the result is summarized in Table 1. The anti-corrosion performances of coatings were investigated quantitatively by evaluating the corrosion rate ( $v_{corr}$ , mm/year) and enhanced protection efficiency ( $P_{EF}$  %). The  $v_{corr}$  was calculated by the following formula:

$$v_{corr}(\text{mm/year}) = \frac{I_{corr}(\text{A cm}^{-2}) \cdot M(\text{g})}{D(\text{g cm}^{-3}) \cdot V} \times 3270$$

where  $I_{corr}$  is the corrosion current density ( $\text{A cm}^{-2}$ ),  $M$  is the molecular mass,  $D$  is the density of carbon steel ( $\text{g cm}^{-3}$ ),  $V$  is the valence (the number of

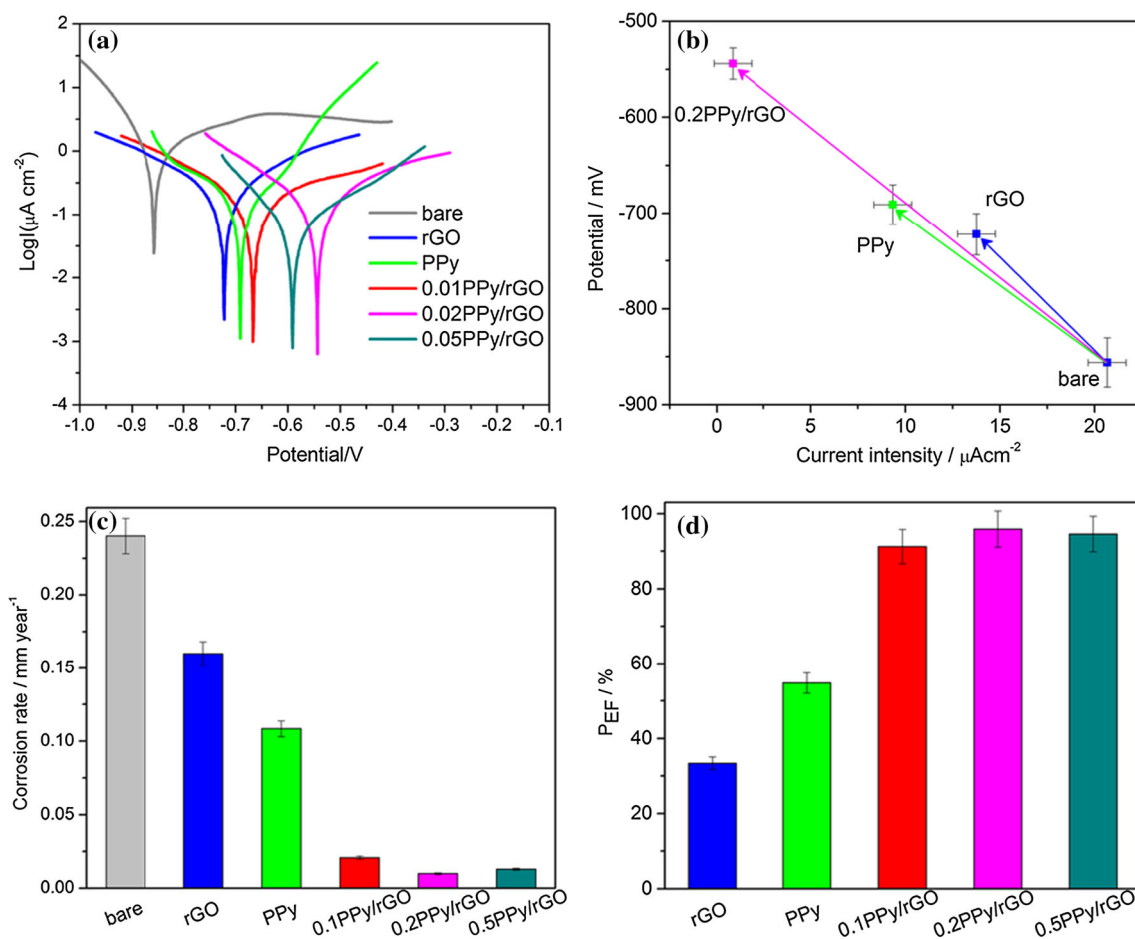


**Figure 4** a Potentiodynamic polarization plots for different coatings after immersing in 3 wt% NaCl solution for 1 h. b  $E_{\text{corr}}$  and  $I_{\text{corr}}$  for coated and bare carbon steel. c Corrosion rates for different coatings extracted from potentiodynamic polarization plots.

**d** Protection efficiency ( $P_{\text{EF}}$  %) for different coatings calculated from potentiodynamic polarization plots [bare carbon steel (gray), carbon steel coated with rGO (blue), PPy (green), 0.01 PPy/rGO (red), 0.02 PPy/rGO (dark cyan) and 0.05 PPy/rGO (magenta)].

**Table 1** Corrosion parameters for coatings on carbon steel in 3 wt% NaCl solution

Coating	$R_p$ ( $\text{k}\Omega \text{ cm}^2$ )	$I_{\text{corr}}$ ( $\mu\text{A cm}^{-2}$ )	$E_{\text{corr}}$ (mV)	$v_{\text{corr}}$ (mm/year)	$P_{\text{EF}}$ (%)
Bare	1.53	20.66	-856	$24.01 \times 10^{-2}$	–
rGO	4.24	13.76	-722	$15.99 \times 10^{-2}$	33.4
PPy	6.33	9.34	-691	$10.85 \times 10^{-2}$	54.8
0.1 PPy/rGO	36.7	1.79	-667	$2.08 \times 10^{-2}$	91.3
0.2 PPy/rGO	66.9	0.85	-544	$0.99 \times 10^{-2}$	95.9
0.5 PPy/rGO	54.1	1.12	-556	$1.30 \times 10^{-2}$	94.6
0.5 PPy/GO	5.52	7.65	-580	$9.20 \times 10^{-2}$	47.1

electrons that were lost during the corrosion reaction) and 3270 is the constant.

$P_{\text{EF}}$  % can be evaluated by the following formula:

$$P_{\text{EF}}\% = \frac{I_{\text{corr}}^0 - I_{\text{corr}}^c}{I_{\text{corr}}^0} \times 100$$

where  $I_{\text{corr}}^0$  is the corrosion current density of bare carbon steel ( $\text{A cm}^{-2}$ ) and  $I_{\text{corr}}^c$  the corrosion current density of carbon steel with coatings ( $\text{A cm}^{-2}$ ).

The  $R_p$  values can be calculated from potentiodynamic polarization plots by the Stern–Geary equation [40]:



$$R_p = \frac{\beta_a \beta_c}{2.303(\beta_a + \beta_c)I_{\text{corr}}}$$

where  $I_{\text{corr}}$  is the corrosion current density and  $\beta_a$  and  $\beta_c$  are the anodic and cathodic slopes ( $\Delta E/\Delta \log I$ ), respectively.

It is well known that the corrosion protection of coating could be evaluated by the values of  $E_{\text{corr}}$ ,  $R_p$ ,  $I_{\text{corr}}$  and  $v_{\text{corr}}$ . The corrosion potential ( $E_{\text{corr}}$ ) and polarization resistance ( $R_p$ ) increased, and corrosion current density ( $I_{\text{corr}}$ ) decreased after the rGO was introduced into the coating, indicating that the PPy/rGO composite coating provided better corrosion protection for the carbon steel. As shown in Fig. 4b and Table 1, the  $E_{\text{corr}}$  values of PPy- and rGO-coated carbon steel shifted toward positive potential, which suggested the decreased corrosion tendency. In addition, compared with the bare carbon steel, the  $E_{\text{corr}}$  values for 0.1, 0.2 and 0.5 PPy/rGO-coated carbon steel shifted to more positive potentials, that is, 189, 312 and 300 mV, respectively, indicating better anti-corrosion performance for PPy/rGO coating than PPy and rGO.

The corrosion current densities ( $I_{\text{corr}}$ ) were calculated by the built-in software of CHI 760D electrochemical workstation. Compared with bare carbon steel, the corrosion currents ( $I_{\text{corr}}$ ) for PPy- and rGO-coated carbon steel were significantly decreased (Fig. 4b), indicating that the rGO and PPy could inhibit the corrosion reaction and reduce the corrosion rate correspondingly. In addition, the decrease in  $I_{\text{corr}}$  from  $20.66 \mu\text{A cm}^{-2}$  for bare carbon steel to  $0.85 \mu\text{A cm}^{-2}$  for 0.2 PPy/rGO-coated carbon steel (Table 1; Fig. 4b) revealed the significantly enhanced anti-corrosion performance for 0.2 PPy/rGO coating. It should be noted that the corrosion rate increased slightly when the concentration of PPy in the electrolyte solution was more than 0.2 M. In other words, as shown in Table 1, the  $I_{\text{corr}}$  of sample PPy/rGO was more than one order lower than that of bare carbon, suggesting that PPy/rGO coating could efficiently protect carbon steel from corrosion. It could not be ignored that the  $I_{\text{corr}}$  of 0.2 PPy/rGO was lower than that of 0.1 and 0.5 PPy/rGO, suggesting that 0.2 PPy/rGO had the best anti-corrosion performance.

As shown in Fig. 4c, the calculated  $v_{\text{corr}}$  for 0.2 PPy/rGO-coated carbon steel ( $0.99 \times 10^{-2} \text{ mm/y}$ ) was about 24 times lower than that for bare carbon steel ( $24.01 \times 10^{-2} \text{ mm/y}$ ). The results of  $v_{\text{corr}}$  and

$P_{\text{EF}}$  % revealed that the PPy/rGO coating exhibited higher anti-corrosion performance than rGO or PPy alone, and the best anti-corrosion performance was obtained when the PPy-doped ratio was 0.2 M. All results proved that the 0.2 PPy/rGO composite coating can be utilized as an efficient barrier for carbon steel protection.

$R_p$  measurement was also carried out for coated carbon steel. As shown in Table 1, the carbon steel coated with 0.2 PPy/rGO showed an  $R_p$  value of  $66.9 \text{ k}\Omega \text{ cm}^2$ , which was higher than that of the bare carbon steel ( $R_p = 1.53 \text{ k}\Omega \text{ cm}^2$ ), rGO ( $R_p = 4.24 \text{ k}\Omega \text{ cm}^2$ ), PPy ( $R_p = 6.33 \text{ k}\Omega \text{ cm}^2$ ), 0.1 PPy/rGO ( $R_p = 36.7 \text{ k}\Omega \text{ cm}^2$ ) and 0.5 PPy/rGO ( $R_p = 54.1 \text{ k}\Omega \text{ cm}^2$ ) coated ones. The protection efficiency ( $P_{\text{EF}}$ ) was also calculated, and the  $P_{\text{EF}}$  of PPy/rGO coating was higher than that of pure PPy or rGO coating. From the result in Fig. 4d, the 0.2 PPy/rGO coating exhibited the highest  $P_{\text{EF}}$  enhancement (95.9%) compared with that of bare carbon steel and the PPy or rGO coating alone yielded only an increase of 54.8 and 33.4 %. In addition, the PPy/rGO coatings exhibited better anti-corrosion performance than polyaniline/graphene composite materials reported previously [38].

### Open-circuit potential ( $E_{\text{ocp}}$ ) and EIS measurements

$E_{\text{ocp}}$  were recorded for bare carbon steel, and 0.1, 0.2, 0.5 coated carbon steel with increasing time in 3 wt% NaCl solution at a constant potential. As shown in Fig. 5a, the curves exhibited a stable and linear behavior for all sample coatings after 24 h in spite of slight fluctuations. It should be noted that the  $E_{\text{ocp}}$  values of all samples decreased during the first 24 h and then remained stable. In addition, the  $E_{\text{ocp}}$  of PPy/rGO-coated carbon steel showed more positive potential than the bare carbon steel. It is well known that  $E_{\text{ocp}}$  directly reflects the corrosion susceptibility [41]. The positive shift in  $E_{\text{ocp}}$  indicated that PPy/rGO coating could protect the carbon steel from being corrosion. In addition, the 0.2 PPy/rGO-coated carbon steel showed the highest  $E_{\text{ocp}}$  value, demonstrating that the best anti-corrosion performance was obtained when the PPy doping concentration was designed at 0.2 M in electrolyte solution.

The anti-corrosion performance of the coatings was also studied using the EIS measurement. The semi-circle curve reflected that electron transfer process

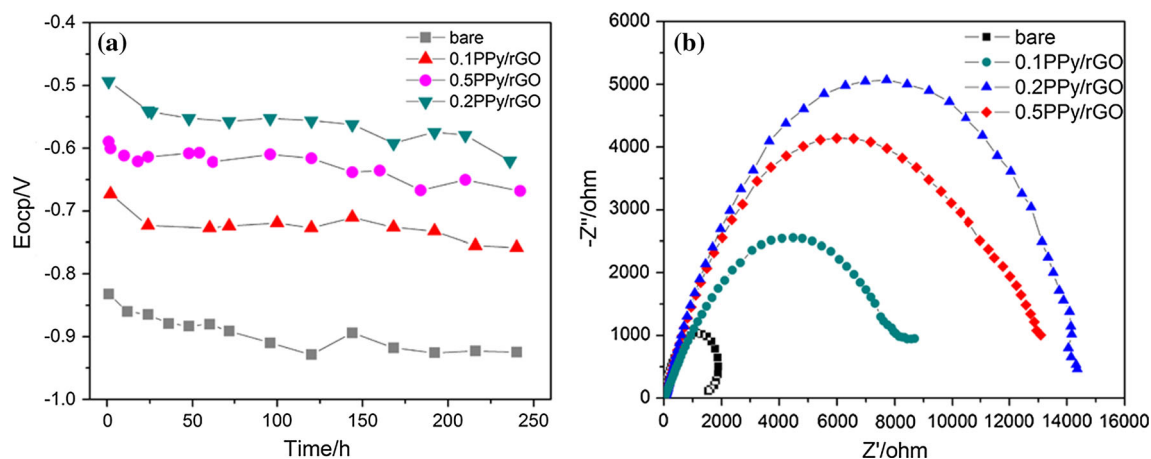


**Figure 5** **a** Open-circuit potential ( $E_{ocp}$ ) versus the immersing time in 3 wt% NaCl solution for bare carbon steel, 0.1, 0.2 and 0.5 PPy/rGO-coated carbon steel. **b** Nyquist plots in 3.5% NaCl solution for bare carbon steel and PPy/rGO-coated carbon steel.

was inhibited on the electrode surface [42]. The diameter of the Nyquist plot could be a parameter to measure the polarization resistance. The semicircle diameters were in the sequence  $0.2 > 0.5 > 0.1$  PPy/rGO  $>$  bare carbon steel. The anti-corrosion properties were enhanced when rGO was doped due to the increase in charge transfer resistance. As shown in Fig. 5b, the  $Z'$  values of bare carbon steel and carbon steel coated with 0.1, 0.5 and 0.2 PPy/rGO composite coatings were 2.0, 8.1, 12.9 and 14.1  $k\Omega\text{ cm}^{-2}$ , respectively. The resulting 0.2 PPy/rGO-coated carbon steel exhibited 7 times higher corrosion resistance than that of bare carbon steel. In other words, the 0.2 PPy/rGO showed the largest radius of the semicircle, indicating the best anti-corrosion performance and lowest electrons transfer rate, which is consistent with the potentiodynamic polarization plots and  $E_{ocp}$  results. Compared with the PPy/rGO curve, an inductive loop in low frequency appeared in the bare carbon steel curve. This inductive loop might be induced by the accelerated pitting corrosion on the surface of carbon steel due to the adsorption of  $\text{Cl}^-$  [42]. The pitting corrosion occurred at the fixed regions of carbon steel by electrochemical reaction until the carbon steel was corroded completely.

### Bode analysis

The 0.2 PPy/rGO-coated carbon steel was chosen to investigate the anti-corrosion performance with immersing time. The 0.2 PPy/rGO-coated carbon steel was immersed in 3% NaCl aqueous solution and was measured by EIS to obtain the Bode phase and

modulus plots as depicted in Fig. 6c and d. The bare carbon steel was also tested for comparison (Fig. 6a, b). In low-frequency region, the charge transfer impedance (corrosion resistance) between anodic and cathodic could be measured by impedance modulus ( $|Z|$ ) [43, 44]. The impedance of 0.2 PPy/rGO (Fig. 6c) was higher than that of the bare carbon steel (Fig. 6a), even though the 0.2 PPy/rGO coating has been immersed into the NaCl solution for 240 h prior to measurement. In addition, the impedance modulus at 0.1 Hz decreased with time for bare carbon steel (Fig. 6b). However, the impedance of 0.2 PPy/rGO-coated carbon steel was relatively stable during the immersion in NaCl solution for 96 h and only decreased slightly with the increasing time up to 240 h, which is probably due to the permeation of  $\text{O}_2$ ,  $\text{H}_2\text{O}$  and  $\text{Cl}^-$ . Larger  $|Z|$  value means less possibility for corrosion to occur; therefore, these Bode modulus measurement results indicated that PPy/rGO coating could efficiently protect carbon steel from corrosion. In a word, the EIS results further illustrated that the PPy/rGO can act as an efficient anti-corrosion coating for carbon steel.

The time constant at high frequency could be assigned to the coating layer, while at low frequency corresponded to a corrosion process at the metal/coating interface [45]. For bare carbon steel, the Bode phase plots displayed two peaks, indicating that there were two time constants in the corrosion process (Fig. 6b). The peak at low frequencies (30 mHz) corresponded to an electrochemical corrosion process at the surface of the carbon steel. The peak intensity increased with the increasing

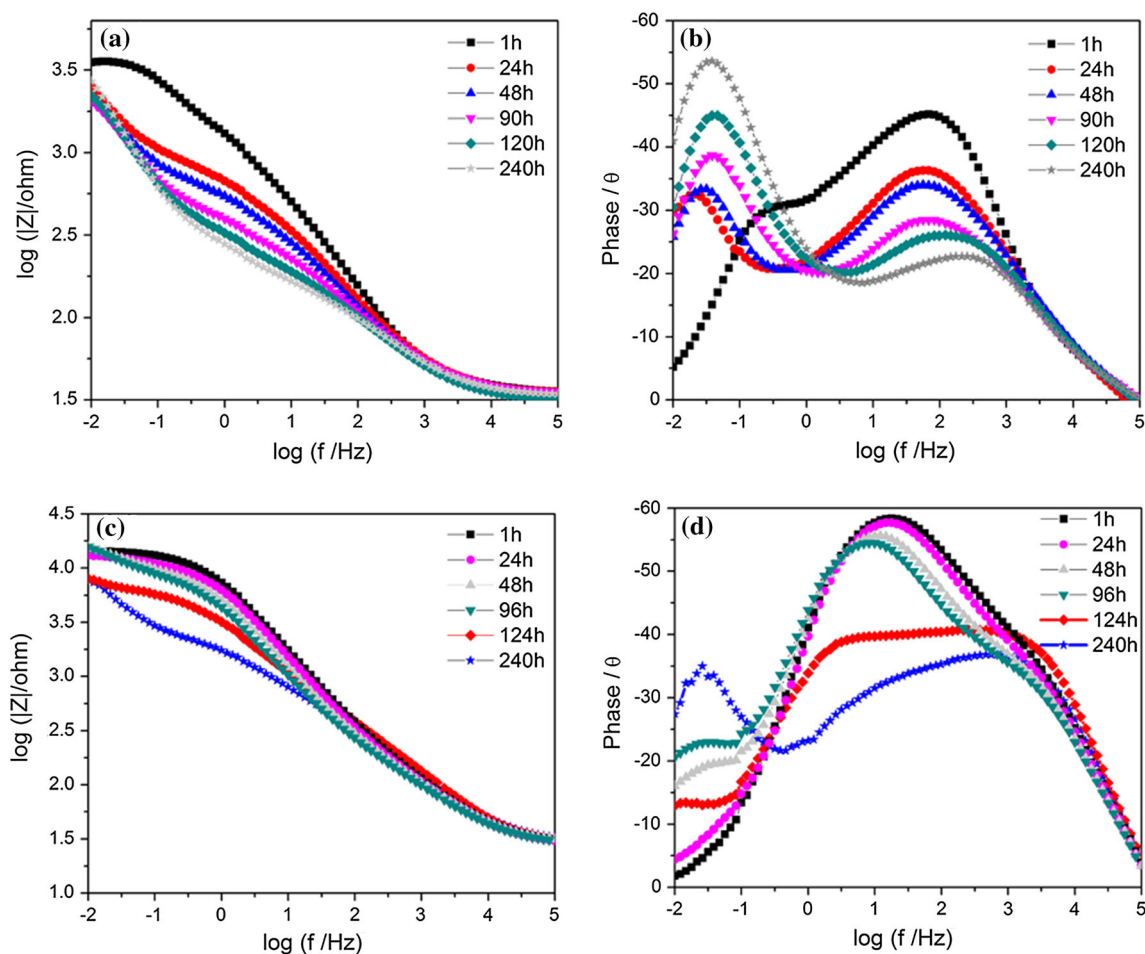


**Figure 6** **a** Bode modulus plots for bare carbon steel, **b** phase plots for bare carbon steel, **c** Bode modulus plots for 0.2 PPy/rGO-coated carbon steel, **d** phase plots for 0.2 PPy/rGO-coated carbon steel against different immersing time up to 240 h.

immersing time, indicating that electrochemical corrosion process occurred. The other peak at intermediate frequencies (60 Hz) could be assigned to the Fe oxide/hydroxide layer, which will be damaged gradually during the corrosion reaction. The Bode phase plot for 0.2 PPy/rGO-coated carbon steel (Fig. 6d) showed two time constants at the first 96 h: one at intermediate frequencies (15 Hz) due to Fe oxide/hydroxide layer and the other one at high frequencies (3.2 kHz) due to the existence of 0.2 PPy/rGO coating. The absence of the low-frequency time constant in the first 24 h demonstrated that no corrosion processes occurred on 0.2 PPy/rGO-coated carbon steel, exhibiting good corrosion protection. With the increasing immersion time, the time constant at intermediate frequencies decreased slightly in 124 h, indicating that the barrier properties of the coating decreased gradually. Although an additional peak at low frequencies (30 mHz) appeared when

0.2 PPy/rGO-coated carbon steel was immersed for 124 h, which was due to the electrochemical corrosion beneath the coating, the time constant at high frequencies due to the PPy/rGO coating still maintained for 240 h of immersion. Only two time constants could be detected (Fig. 6d), indicating that the PPy/rGO was impermeable to corrosive electrolyte and maintained its high anti-corrosion performance throughout the 124-h immersion. However, with the longer immersing time up to 240 h in NaCl solution, the time constant was still visible at high frequencies ( $10^3$  Hz) due to the protection by 0.2 PPy/rGO coating.

### Anti-corrosion mechanism for PPy/rGO nanocomposite coatings

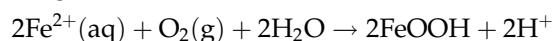
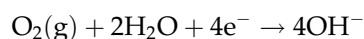
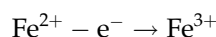
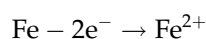
The anti-corrosion mechanisms for PPy-, rGO- or PPy/rGO-coated carbon steel surfaces are shown in

Fig. 7. The combination and interaction between PPy and rGO endow the composite coating with good protection efficiency for carbon steel. The protection mechanism could be explained by the physical barrier effect of the PPy/rGO coatings. The PPy-coated carbon steel surfaces exhibited a loose and thin chrysanthemum-like appearance (Fig. 7a), and the rGO on the surface of carbon steel showed smooth and porous structures (Fig. 7b). The electrolyte could diffuse through the coatings into the surface of carbon steel. As the SEM image shown in Fig. 7c, the rGO was embedded among the PPy to form an ordered nanostructures, which could serve as a barrier to increase the coating impermeability and the tortuosity of the diffusion pathway and correspondingly enhance the anti-corrosion performance. As previously reported, fillers with large filler–matrix interfacial area would help increase the tortuosity of the diffusion pathway [38]. In this aspect, the interfacial area of PPy/rGO coating could be increased due to the attachment of PPy nanostructures on rGO nanosheets to form an ordered structure. The addition of PPy increased the tortuosity of the pathway for the diffusion of  $O_2$ ,  $H_2O$  and  $Cl^-$ , leading to a slower corrosion process for carbon steel.

It has been reported that the conductive coating could not only serve as a barrier for corrosive media, but also an active coating participating the reaction on the surface of the metal [46]. On the other hand,

the conductive coating might induce the formation of a complex oxide passivation, which could terminate the electron transfer required for continued corrosion and then improve the corrosion protective performance of the coating [47]. In addition, it is well known that graphene has large conjugated structure and sufficient electron cloud, so the electrons might be captured by rGO when they are lost from the carbon steel surface. The electron transfer is greatly limited by the coating, and the electrochemical oxidation reactions will be inhibited.

The corrosion and rust formation on carbon steel surface may include several steps, and the oxidation and reduction process can be expressed by the equations as follows:



The existence of  $H_2O$  and  $O_2$  is necessary for the formation of rust and dissolution of carbon steel. If the diffusion of  $H_2O$  and  $O_2$  is inhibited by the coating, the corrosion process could be slow down. Therefore, the prevention of the corrosion of carbon steel can be achieved by increasing the tortuosity of the diffusion pathways for  $H_2O$  and  $O_2$  to reach the surface of the carbon steel. The introduction of rGO

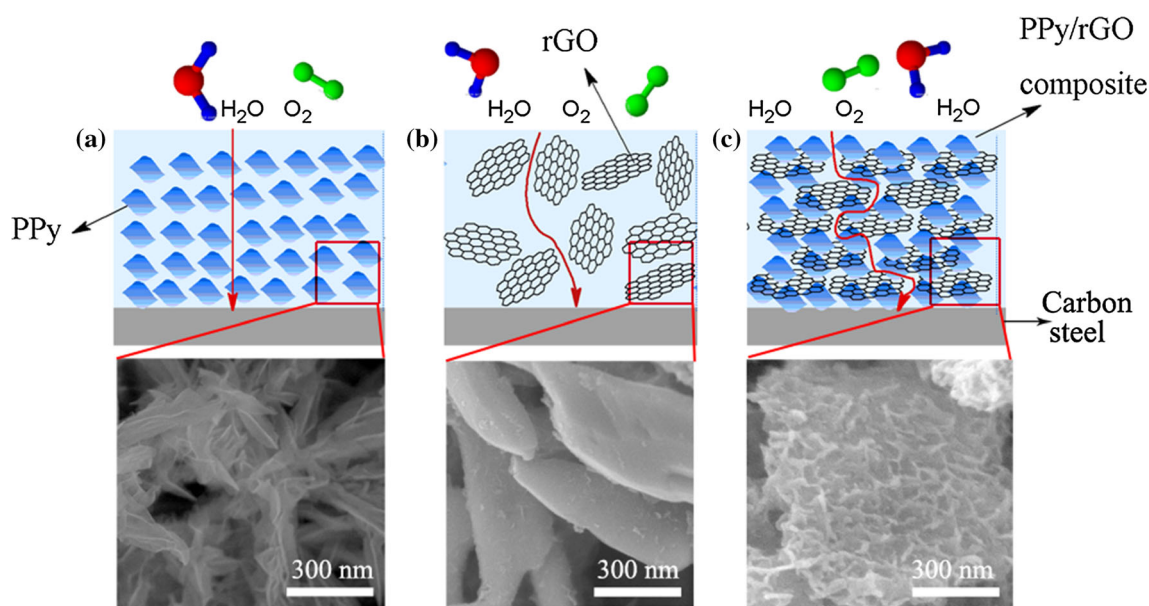


**Figure 7** Schematic representation of the anti-corrosion mechanisms for a PPy-, b rGO- and c PPy/rGO-coated carbon steel surfaces, respectively.



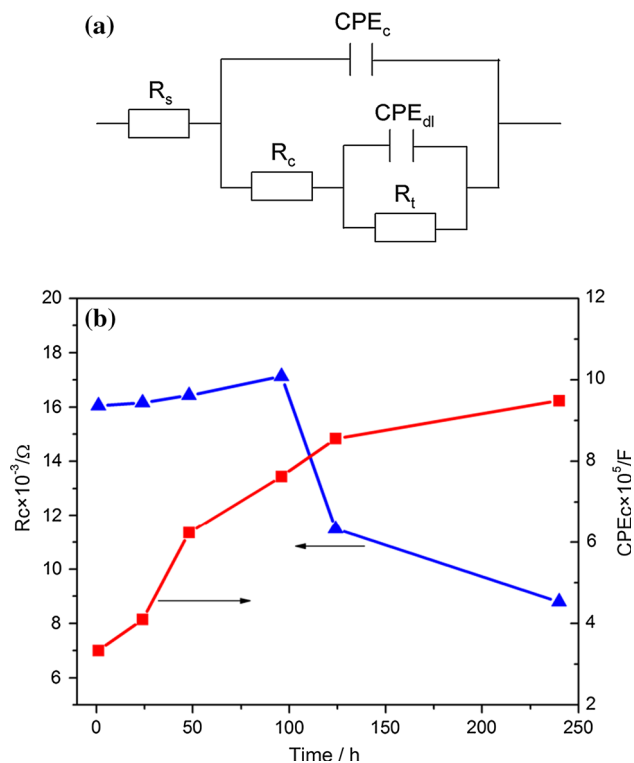


**Figure 8** **a** Equivalent electrical circuit used for the impedance plots fitting of the PPy/rGO coating on carbon steel for different immersion time periods in 3 wt% NaCl solution. **b** Evolution of  $R_c$  (blue) and  $CPE_c$  (red) of the 0.2 PPy/rGO coating.

into PPy created a special ordered structure, which can be used as an efficient barrier for better corrosion protection ability.

### Equivalent electrical circuit analysis

The equivalent electrical circuit that included resistors and capacitors was introduced to quantitatively assess the EIS results and the time-dependent performance of the PPy/rGO coating. In the equivalent circuit depicted in Fig. 8a,  $CPE_{dl}$  is the constant phase element of an electric double-layer capacitance due to the charge accumulation at the interface between the carbon steel and the coating.  $CPE_c$  is the constant phase element related to the coating capacitance.  $R_s$  represents the resistance of the electrolyte solution,  $R_c$  is the resistance of the coating,  $R_t$  represents the polarization resistance or charge transfer resistance in parallel with  $CPE_{dl}$ , reflecting the possibility and degree of difficulty for carbon steel corrosion, and the higher  $R_t$  means the lower corrosion rate.

Table 2 summarizes the values of important electrochemical parameters obtained from the EIS

**Table 2** Electrochemical impedance parameters obtained by simulation of the EIS results for 0.2 PPy/rGO-coated carbon steel

Time (h)	$R_s$ ( $\Omega$ )	$R_c$ ( $\Omega$ )	$CPE_c$ (F)	$R_t$ ( $\Omega$ )	$CPE_{dl}$ (F)
1	28.86	16046	$3.334 \times 10^{-5}$	16435	$1.83 \times 10^{-6}$
24	28.42	16154	$4.094 \times 10^{-5}$	16552	$1.96 \times 10^{-6}$
48	27.93	16424	$6.233 \times 10^{-5}$	15771	$1.85 \times 10^{-6}$
96	29.48	17130	$7.628 \times 10^{-5}$	16328	$2.12 \times 10^{-6}$
124	28.33	9488	$8.557 \times 10^{-5}$	13496	$7.25 \times 10^{-6}$
240	27.97	8796	$9.489 \times 10^{-5}$	10216	$8.22 \times 10^{-6}$

measurement. The anti-corrosion performance of the coating could be reflected by these EIS parameters. It was observed that the  $R_c$  decreased as the immersing time increases, which manifested that the electrolyte has permeated into the inside of the 0.2 PPy/rGO coating. As shown in Fig. 8b, the  $CPE_c$  values increased with the diffusion of the electrolyte solution into the coating. As the electrolyte gradually permeated into the coating, the  $CPE_{dl}$  values increased due to the parallel capacitance characteristics of the coating. It could be seen in Table 2 that the  $R_t$  and  $CPE_{dl}$  values kept steadily in 96 h. The decreased  $R_t$  and increased  $CPE_{dl}$  indicated that the barrier function of the coating attenuated slightly after 124 h. The relatively higher  $CPE_{dl}$  for 0.2 PPy/rGO-coated carbon steel demonstrated a comparatively higher exposure of the carbon steel surface to dissolved oxygen or chloride ions, since the capacitance was directly proportional to the area of the capacitor. Table 2 shows that 0.2 PPy/rGO-coated carbon steel exhibited the better anti-corrosion ability than pure rGO or PPy. However, its anti-corrosion ability decreased obviously within 124 h, which might be due to the generation of small particles as evidenced by the SEM image of the coating sample after 124-h corrosion, as shown in Supporting Information.

### Conclusions

In summary, a facile, efficient and environmentally friendly in situ electrochemical self-assembly method was employed for preparation of ordered PPy/rGO nanocomposite structure onto carbon steel for anti-corrosion application. The synergistic effect between PPy and rGO endows the special structure with an excellent anti-corrosion property for carbon steel. The anti-corrosive behavior of PPy/rGO nanocomposite coatings with different PPy contents was investigated and found that the best anti-corrosion efficiency for

carbon steel was achieved when the weight ratio of PPy and rGO was controlled at 33.5. Potentiodynamic polarization plots, Bode and equivalent electrical circuit were used to investigate the anti-corrosion performance of the nanocomposite. The improved anti-corrosion performance of the PPy/rGO coating could result from the higher contact angles and prolonged diffusion route for O<sub>2</sub> and H<sub>2</sub>O to reach the carbon steel. This special structure exhibited good hydrophobic character, environmentally friendly advantage and efficient anti-corrosion performance for carbon steel and may have tremendous potentiality in naval architecture and ocean engineering.

## Acknowledgement

This work was supported by the Natural Science Foundation of China with Grant (51173087), Qingdao Innovation Leading Expert Program and Taishan Scholars Program.

## Compliance with ethical standards

**Conflict of interest** The authors declare that they have no conflict of interest.

## References

- [1] Chandrasekhar P (1999) *Conducting polymers, fundamentals and applications: a practical approach*. Springer, Berlin
- [2] Goncalves G, Baldissera A, Rodrigues L Jr, Martini E, Ferreira C (2011) Alkyd coatings containing polyanilines for corrosion protection of mild steel. *Synth Met* 161:313–323
- [3] Yao B, Wang G, Ye J, Li X (2008) Corrosion inhibition of carbon steel by polyaniline nanofibers. *Mater Lett* 62:1775–1778
- [4] Zhou C, Zhang Y, Li Y, Liu J (2013) Construction of high-capacitance 3D CoO@polypyrrole nanowire array electrode for aqueous asymmetric supercapacitor. *Nano Lett* 13:2078–2085
- [5] Lange U, Roznyatouskaya NV, Mirsky VM (2008) Conducting polymers in chemical sensors and arrays. *Anal Chim Acta* 614:1–26
- [6] Bai H, Shi G (2007) Gas sensors based on conducting polymers. *Sensors* 7:267–307
- [7] Ocón P, Cristobal AB, Herrasti P, Fatas E (2005) Corrosion performance of conducting polymer coatings applied on mild steel. *Corros Sci* 47:649–662
- [8] Fenelon AM, Breslin CB (2002) The electrochemical synthesis of polypyrrole at a copper electrode: corrosion protection properties. *Electrochim Acta* 47:4467–4476
- [9] Lim Y, Tan YP, Lim HN, Tan WT, Mahnaz M, Talib ZA, Huang NM, Kassim A, Yarmo MA (2013) Polypyrrole/graphene composite films synthesized via potentiostatic deposition. *J Appl Polym Sci* 128:224–229
- [10] Martins J, Reis T, Bazzouai M, Bazzouai E, Martins L (2004) Polypyrrole coatings as a treatment for zinc-coated steel surfaces against corrosion. *Corros Sci* 46:2361–2381
- [11] Iroh JO, Su W (2000) Corrosion performance of polypyrrole coating applied to low carbon steel by an electrochemical process. *Electrochim Acta* 46:15–24
- [12] Ioniță M, Prună A (2011) Polypyrrole/carbon nanotube composites: molecular modeling and experimental investigation as anti-corrosive coating. *Prog Org Coat* 72:647–652
- [13] Lei YH, Sheng N, Hyono A, Ueda M, Ohtsuka T (2013) Electrochemical synthesis of polypyrrole films on copper from phytic solution for corrosion protection. *Corros Sci* 76:302–309
- [14] Krishnamoorthy K, Ramadoss A, Kim SJ (2013) Graphene oxide nanosheets for corrosion-inhibiting coating. *Sci Adv Mater* 5:406–410
- [15] Zhang LL, Zhou R, Zhao X (2010) Graphene-based materials as supercapacitor electrodes. *J Mater Chem* 20:5983–5992
- [16] Stankovich S, Dikin DA, Dommett GHB, Kohlhaas KM, Zimney EJ, Stach EA, Piner RD, Nguyen ST, Ruoff RS (2006) Graphene-based composite materials. *Nature* 442:282–286
- [17] Chen Z, Ren W, Gao L, Liu B, Pei S, Cheng H-M (2011) Three-dimensional flexible and conductive interconnected graphene networks grown by chemical vapour deposition. *Nat Mater* 10:424–428
- [18] Wang Y, Shi Z, Huang Y, Ma Y, Wang C, Chen M, Chen Y (2009) Supercapacitor devices based on graphene materials. *J Phys Chem C* 113:13103–13107
- [19] Bunch JS, Verbridge SS, Alden JS, van der Zande AM, Parpia JM, Craighead HG, McEuen PL (2008) Impermeable atomic membranes from graphene sheets. *Nano Lett* 8:2458–2462
- [20] Sun W, Wang L, Wu T, Pan Y, Liu G (2014) Synthesis of low-electrical-conductivity graphene/pernigraniline composites and their application in corrosion protection. *Carbon* 79:605–614
- [21] Wu Z-S, Ren W, Gao L, Zhao J, Chen Z, Liu B, Tang D, Yu B, Jiang C, Cheng H-M (2009) Synthesis of graphene sheets with high electrical conductivity and good thermal stability by hydrogen arc discharge exfoliation. *ACS Nano* 3:411–417
- [22] Berry V (2013) Impermeability of graphene and its applications. *Carbon* 62:1–10

- [23] Kim KS, Zhao Y, Jang H, Lee SY, Kim JM, Kim KS, Ahn J-H, Kim P, Choi J-Y, Hong BH (2009) Large-scale pattern growth of graphene films for stretchable transparent electrodes. *Nature* 457:706–710
- [24] Singh Raman R, Chakraborty Banerjee P, Lobo DE, Gullapalli H, Sumandasa M, Kumar A, Choudhary L, Tkacz R, Ajayan PM, Majumder M (2012) Protecting copper from electrochemical degradation by graphene coating. *Carbon* 50:4040–4045
- [25] Kirkland N, Schiller T, Medhekar N, Birbilis N (2012) Exploring graphene as a corrosion protection barrier. *Corros Sci* 56:1–4
- [26] Kovtyukhova NI, Ollivier PJ, Martin BR, Mallouk TE, Chizhik SA, Buzaneva EV, Gorchinskiy AD (1999) Layer-by-layer assembly of ultrathin composite films from micron-sized graphite oxide sheets and polycations. *Chem Mater* 11:771–778
- [27] Xing C, Zhang Z, Yu L, Zhang L, Bowmaker GA (2014) Electrochemical corrosion behavior of carbon steel coated by polyaniline copolymers micro/nanostructures. *RSC Adv* 4:32718–32725
- [28] Genzer J, Efimenko K (2006) Recent developments in superhydrophobic surfaces and their relevance to marine fouling: a review. *Biofouling* 22:339–360
- [29] Liu W, Fang Y, Xu P, Lin Y, Yin X, Tang G, He M (2014) Two-step electrochemical synthesis of polypyrrole/reduced graphene oxide composites as efficient Pt-free counter electrode for plastic dye-sensitized solar cells. *ACS Appl Mater Interfaces* 6:16249–16256
- [30] Wang Z, Zhou X, Zhang J, Boey F, Zhang H (2009) Direct electrochemical reduction of single-layer graphene oxide and subsequent functionalization with glucose oxidase. *J Phys Chem C* 113:14071–14075
- [31] Zhang Y, Xiao X, Sun Y, Shi Y, Dai H, Ni P, Hu J, Li Z, Song Y, Wang L (2013) Electrochemical deposition of nickel nanoparticles on reduced graphene oxide film for nonenzymatic glucose sensing. *Electroanalysis* 25:959–966
- [32] Stankovich S, Piner RD, Nguyen ST, Ruoff RS (2006) Synthesis and exfoliation of isocyanate-treated graphene oxide nanoplatelets. *Carbon* 44:3342–3347
- [33] Bora C, Dolui S (2012) Fabrication of polypyrrole/graphene oxide nanocomposites by liquid/liquid interfacial polymerization and evaluation of their optical, electrical and electrochemical properties. *Polymer* 53:923–932
- [34] Bissessur R, Liu PK, Scully SF (2006) Intercalation of polypyrrole into graphite oxide. *Synth Met* 156:1023–1027
- [35] Lim SP, Pandikumar A, Lim YS, Huang NM, Lim HN (2014) In-situ electrochemically deposited polypyrrole nanoparticles incorporated reduced graphene oxide as an efficient counter electrode for platinum-free dye-sensitized solar cells. *Sci Rep* 4:5305/1–5305/7
- [36] Si P, Ding S, Lou X-WD, Kim D-H (2011) An electrochemically formed three-dimensional structure of polypyrrole/graphene nanoplatelets for high-performance supercapacitors. *RSC Adv* 1:1271–1278
- [37] Shao Y, Wang J, Engelhard M, Wang C, Lin Y (2010) Facile and controllable electrochemical reduction of graphene oxide and its applications. *J Phys Chem* 20:743–748
- [38] Chang C-H, Huang T-C, Peng C-W, Yeh T-C, Lu H-I, Hung W-I, Weng C-J, Yang T-I, Yeh J-M (2012) Novel anticorrosion coatings prepared from polyaniline/graphene composites. *Carbon* 50:5044–5051
- [39] Shi X, Nguyen TA, Suo Z, Liu Y, Avci R (2009) Effect of nanoparticles on the anticorrosion and mechanical properties of epoxy coating. *Surf Coat Technol* 204:237–245
- [40] Stern M, Geary AL (1957) Electrochemical polarization I. A theoretical analysis of the shape of polarization curves. *J Electrochem Soc* 104:56–63
- [41] Mišković-Stanković V, Jevremović I, Jung I, Rhee K (2014) Electrochemical study of corrosion behavior of graphene coatings on copper and aluminum in a chloride solution. *Carbon* 75:335–344
- [42] Cao C-N, Zhang J-Q (2002) An introduction to electrochemical impedance spectroscopy. Science, Beijing, p 21
- [43] Zucchi F, Frignani A, Grassi V, TrabANELLI G, Monticelli C (2007) Stannate and permanganate conversion coatings on AZ31 magnesium alloy. *Corros Sci* 49:4542–4552
- [44] He W, Zhu L, Chen H, Nan H, Li W, Liu H, Wang Y (2013) Electrophoretic deposition of graphene oxide as a corrosion inhibitor for sintered NdFeB. *Appl Surf Sci* 279:416–423
- [45] Amirudin A, Thiény D (1995) Application of electrochemical impedance spectroscopy to study the degradation of polymer-coated metals. *Prog Org Coat* 26:1–28
- [46] Wei Y, Wang J, Jia X, Yeh J-M, Spellane P (1995) Polyaniline as corrosion protection coatings on cold rolled steel. *Polymer* 36:4535–4537
- [47] Wessling B (1994) Passivation of metals by coating with polyaniline: corrosion potential shift and morphological changes. *Adv Mater* 6:226–228